Postfilament supercontinuum on 100 m path in air

Olga Kosareva, Nikolay Panov, Daniil Shipilo, Daria Mokrousova, Irina
Nikolaeva, Ekaterina Mitina, Andrew Koribut, Aleksei Reutov, Georgy
Rizaev, Arnaud Couairon, et al.

Postfilament supercontinuum on 100 m path in air

O. Kosareva[1,2,*], N. Panov[1,2], D. Shipilo[1,2], D. Mokrousova[2], I. Nikolaeva[1,2], E. Mitina[1], A. Koribut[2], A. Reutov[2], G. Rizaev[2], A. Couairon[3], A. Houard[4], D. Skryabin[5], A. Saletskiy[1], A. Savel'ev[1,2], L. Seleznev[2], A. Ionin[2], and S. L. Chin[6]

[1] Faculty of Physics and International Laser Center, Lomonosov Moscow State University, Leninskie Gory, Moscow 119991, Russia
[2] P. N. Lebedev Physical Institute of the Russian Academy of Sciences, 53 Leninskiy prospect, Moscow 119991, Russia
[3] CPHT, CNRS, Ecole Polytechnique, Institut Polytechnique de Paris, Route de Saclay, F-91128 Palaiseau, France
[4] LOA, ENSTA Paris, CNRS, Ecole polytechnique, Institut Polytechnique de Paris, 828 Bd des Maréchaux, 91762 Palaiseau, France
[5] Department of Physics, University of Bath, BA2 7AY, Bath, United Kingdom
[6] Center for Optics, Photonics and Lasers (COPL), Laval University, Quebec City, Quebec G1V 0A6, Canada
[*] Corresponding author: kosareva@physics.msu.ru

The pulses at 744 nm with the duration 90 fs, energy 6 mJ and weakly divergent wavefront propagated for more than 100 m and generated a filament followed by unprecedently long high intensity (≥ 1 TW/cm^2) light channel. Over a 20 m long sub-section of this channel the pulse energy is transferred continuously to the infrared wing, forming spectral humps that extend up to the wavelength of 850 nm. From 3D+time carrier-resolved simulations of 100 m pulse propagation, we show that spectral humps indicate the formation of a train of fs pulses appearing at a predictable position in the propagation path. © 2020 Optical Society of America

Supercontinuum laser sources are of ultimate importance for investigation of ultrafast processes in physics, chemistry, biology, and for providing applications for metrology, spectroscopy, and medicine [1–3]. Increase of the width on the infrared side of the spectrum was observed in fibers, where the soliton self-frequency downshift [4–6] can reach hundreds of nm. The Raman response transfers the energy from the short-wavelength to the infrared wing of the soliton spectrum, so that the spectral centre of mass is continuously red shifting with distance. Typical pulse energies in glass-core fibers are in the low nJ range, while using gas-core fibers allows approaching the mJ level [7]. To obtain higher energy infrared pulses in a single-shot, one can use optical parametric amplifiers (OPA) [8] pumped by chirped pulse amplified Ti:Sapphire (Ti:Sa) laser systems providing pulses at 800 nm with TW peak powers [9]. The broadband spectrum of the supercontinuum is usually strongly modulated. This can result in the generation of a femtosecond pulse train [10] both in bulk media [11] and in hollow-core fibers [12].

The frequency conversion distance in free air increases by a factor of 10^3 as compared with crystals in OPA and reaches tens of meters. Spectral measurements performed along the axis of a long-range femtosecond filament at the time of its discovery [13–15] revealed pronounced modulations in the infrared wing of the supercontinuum [13, 14]. These modulations, hereafter called *Ra-*

man humps, were frequency downshifted (Stokes shift) to 795 nm from the fundamental laser wavelength of 775 nm and contained essential fraction of the on-axis radiation. The infrared extension of the on-axis propagating supercontinuum wing generated by 800 nm TW pulses reached 4.5 μm at the level 10^{-5} as compared with the intensity at the fundamental wavelength [16]. Along an indoor several-meters long path in air, a loosely focused 50-fs, 800-nm pulse experienced continuous Stokes shift up to 920 nm [17]. With a 50-fs Ti:Sa collimated pulse, modulated Stokes-shifted spectra were registered behind a 250-μm on-axis aperture placed inside a 4-m cell filled with air or N$_2$ [18, 19]. If the laser central wavelength is 1.03 μm, the Stokes-shifted spectrum reaches 1.15 μm [20]. These observations of Stokes shift raise several questions. First, on whether the downshift only occurs along the high-intensity region of the filament [21] supporting a plasma channel, or persists further on in the ionization-free zone [22]. Second, how to quantitatively predict the formation of Raman humps along a path length of several hundreds of meters from available measurements over shorter distances [17–20, 23–25]. So far, the longest path for the continuous Stokes shift measurement of Ti:Sa pulses propagating in air was ∼9 m [17], while applications such as the remote detection of bioaerosols [26] would benefit from the availability of broadband Stokes-shifted pulses at hundreds of meters from the source.

In this work, we measure and simulate the generation of spectral Raman humps from 744 to 850 nm during propagation of a 90-fs, 6-mJ laser pulse along a 100-m path in air. At such a low energy and long distance, the plasma channel was detected indirectly through the presence of white light conical emission at 100 m and confirmed by simulations with carrier wave resolution of nonlinear pulse propagation and filamentation over the ∼100-m long path. We show that Raman humps are recurrently generated beyond the filament in a 20 m long *Stokes zone*. Each hump appears at a separate location with a predictable central frequency, thus providing a train of Stokes shifted fs pulses.

In our experiments (Fig. 1), laser pulses with central wavelength of $\lambda_0 = 744$ nm, energy of ∼6 mJ, full width at half-maximum (FWHM) duration of ∼90 fs and diameter of ∼8 mm at e^{-1} fluence level were delivered by the Ti:Sa laser facility Start-
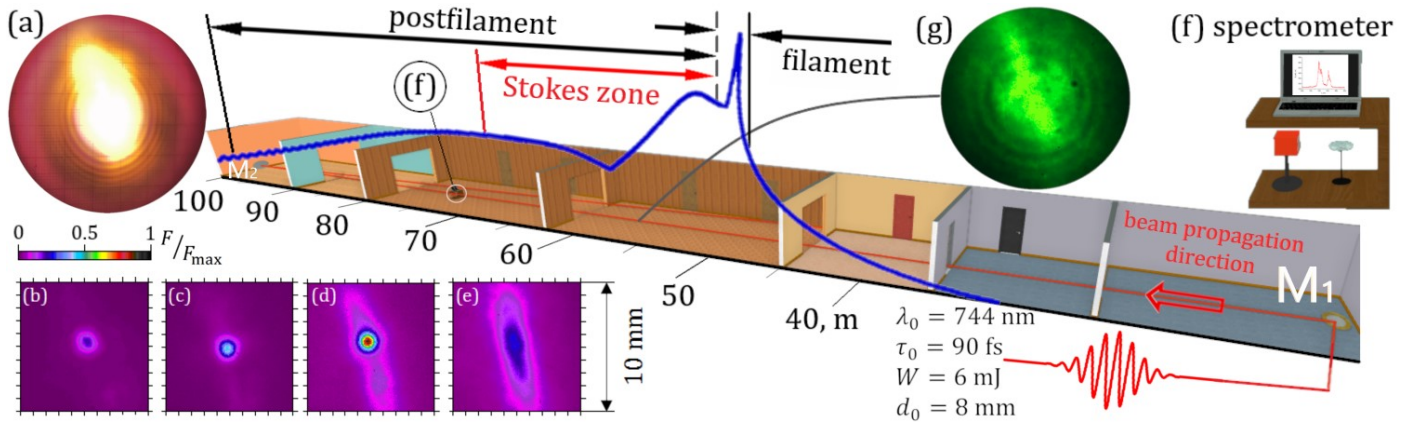
Fig. 1. Sketch of the experiment in the corridor with the trolley (f) equipped with spectrometer and CCD camera. Blue curve is variation of the simulated peak intensity vs. propagation distance from the compressor output. (a) Conical emission on the far wall of the corridor. Measured transverse fluence distributions at (b) 100 m, (c) 80 m, (d) 50 m, (e) 40 m. (g) Transverse beam profile observed at 56 m using low-pass spectral filters to increase the contrast of rings.

248 from Avesta Project Ltd located in a clean room. The pulses were sent to a ∼100 m corridor through a hole in the wall and adjusted by a high reflectivity mirror M1 (Fig. 1). The beam pattern after the mirror M1 was elliptical in shape and slightly divergent with geometrical focus of −50 m. Another mirror M2 reflected the beam at the end of the corridor and elongated the path to ∼150 m. The registration system was maintained on a trolley to move the equipment along the corridor starting from the mirror M1 at ∼11 m from the compressor output. Light channel characterization was performed by a spectrometer Avesta ASP-150 (spectral resolution of 0.1 nm) and CCD-camera Ophir Spiricon SP620U. Before entering the aperture of the spectrometer the radiation was reflected by a wedge. The angle of reflection varied along the path to attenuate the signal. So, the spectra had different calibration along the corridor. At each position along the propagation path we recorded 20 to 30 on-axis spectra with the developed infrared wing, while the conical emission did not enter the spectrometer. The beam patterns were registered using a CCD camera [Fig. 1(b)–(e)] and digitally processed to retrieve the diameter along the 100 m path [Fig. 2(a), filled circles].

The initial pulse peak power of 67 GW is high enough to produce a single filament. The parameters of the experiment are close to the ones used in earlier corridor experiments [13–15] except for the pulse duration, which was shorter than 150 fs [14] or 200 fs [13, 15]. This allowed us to measure higher energy in the infrared wing and to observe the novel feature of recurrent generation of separate Raman humps. We monitored the infrared wing with high longitudinal resolution along the propagation path, using the valuable information on the nonmonotonic fraction of the total pulse energy (refocusing phenomenon) in the core of a long single filament [15]. A single filament started to form at the distance of 45–50 m from the compressor, where the beam diameter shrank down to 920 μm [Fig. 2(a)] producing a unimodal transverse fluence distribution [27] sustained up to ∼100 m [cf. Fig. 1(b) and Fig. 1(c)]. Characteristic beam patterns are shown before [40 m, Fig. 1(e)] and after [50 m, Fig. 1(d)] the plasma column accompanying the filament. Appearance of a round conical emission of several cm in diameter at $z = 100$ m [Fig. 1(a)] proves the presence of a single filament [14, 28]. The rings in the beam fluence background [Fig. 1(g)] give additional evidence of the plasma channel generated by the filament [29]. Simulations reveal a 0.3 m long plasma string [Fig. 2(a), inset].

The advantage of the slightly divergent beam is the nice longitudinal resolution of the pulse spectrum transformation along the path. The burst of the supercontinuum is associated with the self-focusing collapse [13, 14, 30, 31], which in our experiment is identified through the beam diameter decrease at 48 m [Fig. 2(a)]. After the collapse ($z > 48$ m) we observe the occurrence of the on-axis spectral broadening from 744 to 820 nm over a distance of 20 m [Fig. 2(c), open circles], accompanied by the emergence of a new spectral peak (hump) every 3–4 m of propagation [Fig. 3(a)]. Each subsequent hump is shifted by ∼20 nm to the infrared as compared with the previous one [Fig. 3(a), 55–70 m]. In Fig. 3(a) the low level of spectral intensity at $\lambda_0 = 744$ nm at $z < 70$ m is because we selected the spectra, for which the Raman humps were best pronounced. Then the spectral intensity was normalized to the maximum of the hump with the longest central wavelength. The spectrum at 90 m shown in Fig. 3(c) reveals four peaks, whose central wavelengths remain unchanged up to 150 m.

Numerical simulations on a 100-m path were carried out to quantify the peak intensity in the filament and postfilamentation channel as well as the temporal profile of the pulse with the expectation of femtosecond pulse train predicted in Ref. [12]. We use the Forward Maxwell equation (FME, paraxial propagation equation for carrier-wave-resolved fields [32, 33]) in axially-symmetrical geometry $(t, r) + z$ due to the moderate pulse power in our experiment. The nonlinear source term in FME includes transient photocurrent as well as the third-order instantaneous and delayed [34] nonlinearities. The Kerr coefficient $n_2 = 10^{-19}$ cm^2/W is chosen according to the experiment [35] and *ab initio* calculations [36]. The simulations covering propagation distances larger than 100 m require adapted grids to resolve highly nonlinear dynamics. Our numerical grid reliably resolves the third harmonic, with 6 nodes per third-harmonic period (temporal resolution of 0.15 fs). The temporal domain of ∼40 ps is larger than the group walk-off between the third harmonic and the pump ∼300 fs/m×100 m, and z-step is 0.5 cm or smaller to provide at least 6 steps per phase matching length of ∼2.7 cm [33]. In the transverse domain r we start from a beam with the radius of 0.4 cm. We choose the r-domain as large as 4 cm with the best resolution of 4 μm in the central area with the radius of 0.4 cm, increasing to the edge of the domain as required to both resolve nonlinearity within
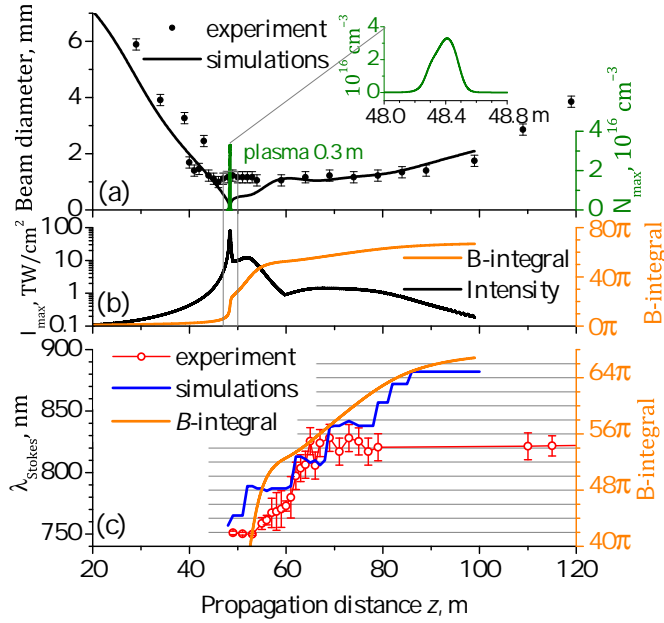
Fig. 2. (a) Beam diameter FWe^{-1}M vs. propagation distance z in the experiment (filled circles) and simulations (black curve). Green sharp curve and the inset represent the simulated plasma density. (b) Simulated peak intensity I_{max} (black curve, left axis) and B-integral (orange curve, right axis) vs. z. (c) Experimental (open circles) and simulated (blue curve) position λ_{Stokes} (left axis) of the longest-wavelength maximum in the spectrum. Orange curve is B-integral from (b).

the filament and capture the wide conical emission, propagating at an angle of ~1 mrad to the optical axis. At the distance $z = 100$ m the fluence level at the boundary $r = 4$ cm is less than 10^{-5} of the maximum value at $r = 0$. At shorter distances $z \leq 80$ m this ratio is well below 10^{-10}. The numerical grid was $2^{18}(t) \times 1450(r) \times 25\,000(z)$, but a single z-step needs to be kept in computer memory for space-marching, so our solver requires 24 GByte RAM. A single run over 100-m path takes ~10 days for parallel 40 threads on two Intel Xeon E5-2698 processors.

The simulations summarized in Figs. 2, 3 provide a good agreement with measured beam diameters, central wavelengths and extent of Raman humps, as well as with their appearance location in the Stokes zone (Fig. 3). In simulations, the advance of the humps to the infrared can be simply quantified according to the self-phase modulation in a plane wave [37]. Simulations indicate that the plasma channel is 0.3–0.4 m long [Fig. 2(a), inset], ~50 times shorter than the Stokes zone, and acts almost as a point source for the high-frequency side of the supercontinuum.

The simulations allow us to follow along a 100-m path the peak intensity I_{max} [Fig. 2(b), black curve] which is 80 TW/cm^2 in the plasma string [38], ~2 TW/cm^2 in the Stokes zone 54–74 m and decreases to 0.2 TW/cm^2 at 100 m. The oscillations in $I_{max}(z)$ at $z > 70$ m appear due to the interference between 744-nm pump and multiple subpulses (Fig. 4) flowing over it due to group velocity difference. We calculate the B-integral $B(z) = (2\pi n_2/\lambda_0) \times \int_0^z I_{max}(z')dz'$ [Fig. 2, orange, Fig. 3(b), black curve], which exhibits a quasilinear dependence in the Stokes zone, and get an increase of ~2π for every newly emerging Raman hump [Fig. 3(b)]. Using $I_{max} \approx 2$ TW/cm^2 the formation distance of a new Raman hump is estimated as $\Delta z = \lambda_0/(n_2 I_{max}) \approx 3$ m in agreement with the experiment.
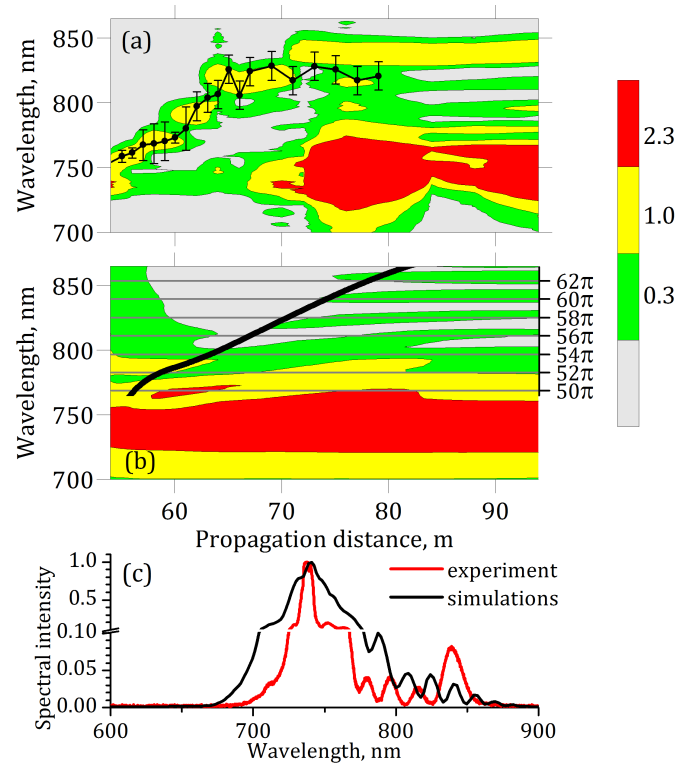

Fig. 3. Resolved over the distance z spectra of the Stokes side of the supercontinuum in the experiment (a) and simulations (b) and their slice at 90 m (c). Black circles in (a) repeat the measured dependence of *averaged* $\lambda_{Stokes}(z)$ from Fig. 2(c); it differs slightly from the color map as the latter is based on *single-shot* spectra. Black curve (right axis) in (b) shows the simulated dependence of B-integral on z.

In simulations, the infrared wing of the supercontinuum ranging from 777 to 860 nm contains an energy of 0.27 mJ (4.5% of 6 mJ). The energy within each hump is relatively large and equal to 20–120 μJ at 90 m. The periodic multi-hump structure in spectrum can form a train of fs pulses in the time domain [10], as observed during propagation of a two-color pulse in a cuvette filled with tenuous D$_2$ [11] and in a hollow-core fused silica fiber filled with 3-bar SF$_6$ [12]. In our experiment the postfilament preserves the transverse mode with high intensity for more than 20 m similar to a hollow fiber. This extended interaction region ensures the observation of the periodic multi-hump spectrum.

We explored numerically the temporal profile of the pulse. A clearly pronounced train of 15-fs pulses appears at 80 m in the pulse front [Fig. 4(a), 4(b), $-140 < t < -80$ fs]. We applied Fourier transform to this selected temporal interval after zero-padding the rest of the grid points [Fig. 4(b), red curve]. The infrared multi-hump structure corresponds to the pulse train [Fig. 4(c)]. The shape of our measured spectrum and its agreement with the simulated one (Fig. 3) suggests that the pulse train is formed in the Stokes zone. Thus, the long-range postfilament is characterized by a unimodal infrared core [23, 24], which carries out the quasiperiodic multi-hump structure we observed in the spectral domain. The corresponding distribution of the light field in the temporal domain contains a femtosecond pulse train.

The observed multi-hump structure is useful for the atmospheric applications where a long distance propagation of the filament is required and only a remote control of the pulse on
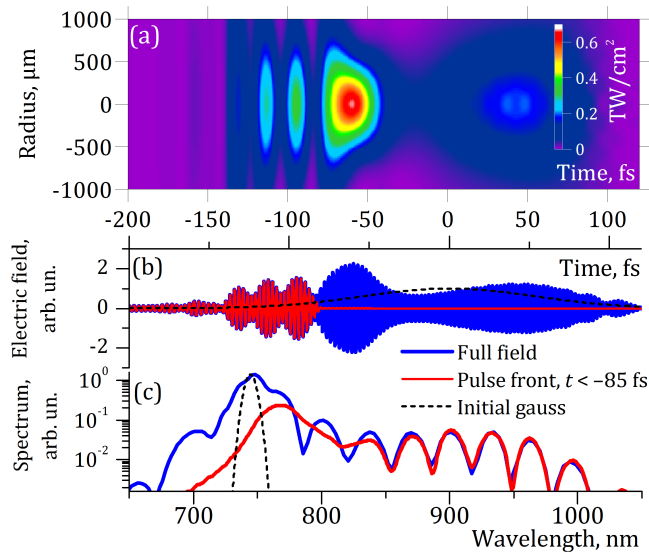
Fig. 4. Simulated (a) spatio-temporal distribution of the pulse intensity, (b) on-axis light field and (c) integrated over beam spectrum of the whole pulse (blue curve) and of the pulse train in its front ($t < -85$ fs, red curve) at $z = 80$ m.

target can be realized [3]. There are easier ways of producing red-shifted pulses in the laboratory [4, 5, 8], but their intensity and spectrum might change essentially after nonlinear propagation over hundreds of meters in air. In our experiment the formation distance of each new Raman hump is predictable and can be remotely controlled by means of the initial beam wavefront curvatures and pulse chirp [3, 39]. The spectral content of the humps [Fig. 3(c)] covers the ro-vibrational transitions of H_2O in the range 828–832 nm [39].

In conclusion, we demonstrate that filamentation in air of moderately powerful 90 fs, 6 mJ, 744 nm laser pulses with weakly divergent wavefront constitutes a source of femtosecond pulse train featured by a Stokes shifted multi-hump spectrum. Each Raman hump appears separately in a given range of the 20 m long Stokes zone and corresponds to the Stokes-shifted pulse with a predefined wavelength that can reach 850 nm.

Disclosures. The authors declare that there are no conflicts of interest related to this article.

REFERENCES

1. F. J. Duarte, *Tunable laser applications*, vol. 150 (CRC press, 2008).
2. T. Udem, R. Holzwarth, and T. W. Hänsch, Nature **416**, 233 (2002).
3. J. Kasparian, M. Rodríguez, G. Méjean, J. Yu, E. Salmon, H. Wille, R. Bourayou, S. Frey, Y.-B. André, A. Mysyrowicz, R. Sauerbrey, J.-P. Wolf, and L. Wöste, Science **301**, 61 (2003).
4. F. M. Mitschke and L. F. Mollenauer, Opt. Lett. **11**, 659 (1986).
5. N. Ishii, C. Y. Teisset, S. Köhler, E. Serebryannikov, T. Fuji, T. Metzger, F. Krausz, A. Baltuška, and A. Zheltikov, Phys. Rev. E **74**, 036617 (2006).
6. D. V. Skryabin and A. V. Gorbach, Rev. Mod. Phys. **82**, 1287 (2010).
7. J. C. Travers, T. F. Grigorova, C. Brahms, and F. Belli, Nat. Photonics **13**, 547 (2019).
8. G. Cerullo and S. De Silvestri, Rev. Sci. Instrum. **74**, 1 (2003).
9. D. Strickland and G. Mourou, Opt. Commun. **55**, 447 (1985).
10. S. Yoshikawa and T. Imasaka, Opt. Commun. **96**, 94 (1993).
11. A. V. Sokolov, D. R. Walker, D. Yavuz, G. Yin, and S. Harris, Phys. Rev. Lett. **87**, 033402 (2001).
12. F. Turner, A. Trottier, D. Strickland, and L. Losev, Opt. Commun. **270**, 419 (2007).
13. A. Braun, G. Korn, X. Liu, D. Du, J. Squier, and G. Mourou, Opt. Lett. **20**, 73 (1995).
14. E. Nibbering, P. Curley, G. Grillon, B. Prade, M. Franco, F. Salin, and A. Mysyrowicz, Opt. Lett. **21**, 62 (1996).
15. A. Brodeur, C. Chien, F. Ilkov, S. Chin, O. Kosareva, and V. Kandidov, Opt. Lett. **22**, 304 (1997).
16. J. Kasparian, R. Sauerbrey, D. Mondelain, S. Niedermeier, J. Yu, J.-P. Wolf, Y.-B. André, M. Franco, B. Prade, S. Tzortzakis, A. Mysyrowicz, M. Rodriguez, H. Wille, and L. Wöste, Opt. Lett. **25**, 1397 (2000).
17. Y. Chen, F. Théberge, C. Marceau, H. Xu, N. Aközbek, O. Kosareva, and S. Chin, Appl. Phys. B **91**, 219 (2008).
18. E. Nibbering, G. Grillon, M. A. Franco, B. S. Prade, and A. Mysyrowicz, J. Opt. Soc. Am. B **14**, 650 (1997).
19. D. Uryupina, N. Panov, M. Kurilova, A. Mazhorova, R. Volkov, S. Gorgutsa, O. Kosareva, and A. Savel'ev, Appl. Phys. B **110**, 123 (2013).
20. A. Mitrofanov, A. Voronin, D. Sidorov-Biryukov, G. Andriukaitis, T. Flöry, A. Pugžlys, A. Fedotov, J. Mikhailova, V. Y. Panchenko, A. Baltuška, and A. Zheltikov, Opt. Lett. **39**, 4659 (2014).
21. N. A. Panov, D. E. Shipilo, V. A. Andreeva, D. S. Uryupina, A. B. Savel'ev, O. G. Kosareva, and S. L. Chin, Appl. Phys. B **120**, 383 (2015).
22. G. Méchain, A. Couairon, Y.-B. André, C. D'Amico, M. Franco, B. Prade, S. Tzortzakis, A. Mysyrowicz, and R. Sauerbrey, Appl. Phys. B **79**, 379 (2004).
23. J.-F. Daigle, O. Kosareva, N. Panov, T.-J. Wang, S. Hosseini, S. Yuan, G. Roy, and S. L. Chin, Opt. Commun. **284**, 3601 (2011).
24. J.-F. Daigle, T.-J. Wang, S. Hosseini, S. Yuan, G. Roy, and S. L. Chin, Appl. Opt. **50**, 6234 (2011).
25. M. Durand, A. Houard, B. Prade, A. Mysyrowicz, A. Durécu, B. Moreau, D. Fleury, O. Vasseur, H. Borchert, K. Diener, R. Schmitt, F. Théberge, M. Chateauneuf, J.-F. Daigle, and J. Dubois, Opt. Express **21**, 26836 (2013).
26. H. Xu, G. Méjean, W. Liu, Y. Kamali, J.-F. Daigle, A. Azarm, P. Simard, P. Mathieu, G. Roy, J.-R. Simard, and S. Chin, Appl. Phys. B **87**, 151 (2007).
27. W. Liu and S. L. Chin, Phys. Rev. A **76**, 013826 (2007).
28. O. Kosareva, J.-F. Daigle, N. Panov, T. Wang, S. Hosseini, S. Yuan, G. Roy, V. Makarov, and S. L. Chin, Opt. Lett. **36**, 1035 (2011).
29. S. Chin, N. Aközbek, A. Proulx, S. Petit, and C. Bowden, Opt. Commun. **188**, 181 (2001).
30. O. Kosareva, V. Kandidov, A. Brodeur, C. Chien, and S. Chin, Opt. Lett. **22**, 1332 (1997).
31. P. Corkum and C. Rolland, IEEE J. Quant. Electron. **25**, 2634 (1989).
32. M. Kolesik and J. V. Moloney, Phys. Rev. E **70**, 036604 (2004).
33. N. A. Panov, D. E. Shipilo, A. M. Saletsky, W. Liu, P. G. Polynkin, and O. G. Kosareva, Phys. Rev. A **100**, 023832 (2019).
34. P. A. Oleinikov and V. T. Platonenko, Laser Phys. **3**, 618 (1993).
35. W. Liu and S. L. Chin, Opt. Express **13**, 5750 (2005).
36. J. M. Brown, A. Couairon, and M. B. Gaarde, Phys. Rev. A **97**, 063421 (2018).
37. S. A. Akhmanov, V. A. Vysloukh, and A. S. Chirkin, *Optics of femtosecond laser pulses* (1988).
38. J. Kasparian, R. Sauerbrey, and S. L. Chin, Appl. Phys. B **71**, 877 (2000).
39. P. Rairoux, H. Schillinger, S. Niedermeier, M. Rodriguez, F. Ronneberger, R. Sauerbrey, B. Stein, D. Waite, C. Wedekind, H. Wille, L. Wöste, and C. Ziener, Appl. Phys. B **71**, 573 (2000).

FULL REFERENCES

1. F. J. Duarte, *Tunable laser applications*, vol. 150 (CRC press, 2008).
2. T. Udem, R. Holzwarth, and T. W. Hänsch, "Optical frequency metrology," Nature **416**, 233–237 (2002).
3. J. Kasparian, M. Rodríguez, G. Méjean, J. Yu, E. Salmon, H. Wille, R. Bourayou, S. Frey, Y.-B. André, A. Mysyrowicz, R. Sauerbrey, J.-P. Wolf, and L. Wöste, "White-light filaments for atmospheric analysis," Science **301**, 61–64 (2003).
4. F. M. Mitschke and L. F. Mollenauer, "Discovery of the soliton self-frequency shift," Opt. Lett. **11**, 659–661 (1986).
5. N. Ishii, C. Y. Teisset, S. Köhler, E. Serebryannikov, T. Fuji, T. Metzger, F. Krausz, A. Baltuška, and A. Zheltikov, "Widely tunable soliton frequency shifting of few-cycle laser pulses," Phys. Rev. E **74**, 036617 (2006).
6. D. V. Skryabin and A. V. Gorbach, "Colloquium: Looking at a soliton through the prism of optical supercontinuum," Rev. Mod. Phys. **82**, 1287–1299 (2010).
7. J. C. Travers, T. F. Grigorova, C. Brahms, and F. Belli, "High-energy pulse self-compression and ultraviolet generation through soliton dynamics in hollow capillary fibres," Nat. Photonics **13**, 547 (2019).
8. G. Cerullo and S. De Silvestri, "Ultrafast optical parametric amplifiers," Rev. Sci. Instrum. **74**, 1–18 (2003).
9. D. Strickland and G. Mourou, "Compression of amplified chirped optical pulses," Opt. Commun. **55**, 447–449 (1985).
10. S. Yoshikawa and T. Imasaka, "A new approach for the generation of ultrashort optical pulses," Opt. Commun. **96**, 94–98 (1993).
11. A. V. Sokolov, D. R. Walker, D. Yavuz, G. Yin, and S. Harris, "Femtosecond light source for phase-controlled multiphoton ionization," Phys. Rev. Lett. **87**, 033402 (2001).
12. F. Turner, A. Trottier, D. Strickland, and L. Losev, "Transient multifrequency raman generation in sf6," Opt. Commun. **270**, 419–423 (2007).
13. A. Braun, G. Korn, X. Liu, D. Du, J. Squier, and G. Mourou, "Self-channeling of high-peak-power femtosecond laser-pulses in air," Opt. Lett. **20**, 73 (1995).
14. E. Nibbering, P. Curley, G. Grillon, B. Prade, M. Franco, F. Salin, and A. Mysyrowicz, "Conical emission from self-guided femtosecond pulses in air," Opt. Lett. **21**, 62–64 (1996).
15. A. Brodeur, C. Chien, F. Ilkov, S. Chin, O. Kosareva, and V. Kandidov, "Moving focus in the propagation of ultrashort laser pulses in air," Opt. Lett. **22**, 304–306 (1997).
16. J. Kasparian, R. Sauerbrey, D. Mondelain, S. Niedermeier, J. Yu, J.-P. Wolf, Y.-B. André, M. Franco, B. Prade, S. Tzortzakis, A. Mysyrowicz, M. Rodriguez, H. Wille, and L. Wöste, "Infrared extension of the supercontinuum generated by femtosecond terawatt laser pulses propagating in the atmosphere," Opt. Lett. **25**, 1397–1399 (2000).
17. Y. Chen, F. Théberge, C. Marceau, H. Xu, N. Aközbek, O. Kosareva, and S. Chin, "Observation of filamentation-induced continuous self-frequency down shift in air," Appl. Phys. B **91**, 219–222 (2008).
18. E. Nibbering, G. Grillon, M. A. Franco, B. S. Prade, and A. Mysyrowicz, "Determination of the inertial contribution to the nonlinear refractive index of air, n2, and o2 by use of unfocused high-intensity femtosecond laser pulses," J. Opt. Soc. Am. B **14**, 650–660 (1997).
19. D. Uryupina, N. Panov, M. Kurilova, A. Mazhorova, R. Volkov, S. Gorgutsa, O. Kosareva, and A. Savel'ev, "3D raman bullet formed under filamentation of femtosecond laser pulses in air and nitrogen," Appl. Phys. B **110**, 123–130 (2013).
20. A. Mitrofanov, A. Voronin, D. Sidorov-Biryukov, G. Andriukaitis, T. Flöry, A. Pugžlys, A. Fedotov, J. Mikhailova, V. Y. Panchenko, A. Baltuška, and A. Zheltikov, "Post-filament self-trapping of ultrashort laser pulses," Opt. Lett. **39**, 4659–4662 (2014).
21. N. A. Panov, D. E. Shipilo, V. A. Andreeva, D. S. Uryupina, A. B. Savel'ev, O. G. Kosareva, and S. L. Chin, "Robust near-infrared light bullet in 800-nm femtosecond light filaments in air," Appl. Phys. B **120**, 383–387 (2015).
22. G. Méchain, A. Couairon, Y.-B. André, C. D'Amico, M. Franco, B. Prade, S. Tzortzakis, A. Mysyrowicz, and R. Sauerbrey, "Long-range self-channeling of infrared laser pulses in air: a new propagation regime without ionization," Appl. Phys. B **79**, 379–382 (2004).
23. J.-F. Daigle, O. Kosareva, N. Panov, T.-J. Wang, S. Hosseini, S. Yuan, G. Roy, and S. L. Chin, "Formation and evolution of intense, post-filamentation, ionization-free low divergence beams," Opt. Commun. **284**, 3601–3606 (2011).
24. J.-F. Daigle, T.-J. Wang, S. Hosseini, S. Yuan, G. Roy, and S. L. Chin, "Dynamic behavior of postfilamentation raman pulses," Appl. Opt. **50**, 6234–6238 (2011).
25. M. Durand, A. Houard, B. Prade, A. Mysyrowicz, A. Durécu, B. Moreau, D. Fleury, O. Vasseur, H. Borchert, K. Diener, R. Schmitt, F. Théberge, M. Chateauneuf, J.-F. Daigle, and J. Dubois, "Kilometer range filamentation," Opt. Express **21**, 26836–26845 (2013).
26. H. Xu, G. Méjean, W. Liu, Y. Kamali, J.-F. Daigle, A. Azarm, P. Simard, P. Mathieu, G. Roy, J.-R. Simard, and S. Chin, "Remote detection of similar biological materials using femtosecond filament-induced breakdown spectroscopy," Appl. Phys. B **87**, 151–156 (2007).
27. W. Liu and S. L. Chin, "Abnormal wavelength dependence of the self-cleaning phenomenon during femtosecond-laser-pulse filamentation," Phys. Rev. A **76**, 013826 (2007).
28. O. Kosareva, J.-F. Daigle, N. Panov, T. Wang, S. Hosseini, S. Yuan, G. Roy, V. Makarov, and S. L. Chin, "Arrest of self-focusing collapse in femtosecond air filaments: higher order kerr or plasma defocusing?" Opt. Lett. **36**, 1035–1037 (2011).
29. S. Chin, N. Aközbek, A. Proulx, S. Petit, and C. Bowden, "Transverse ring formation of a focused femtosecond laser pulse propagating in air," Opt. Commun. **188**, 181–186 (2001).
30. O. Kosareva, V. Kandidov, A. Brodeur, C. Chien, and S. Chin, "Conical emission from laser–plasma interactions in the filamentation of powerful ultrashort laser pulses in air," Opt. Lett. **22**, 1332–1334 (1997).
31. P. Corkum and C. Rolland, "Femtosecond continua produced in gases," IEEE J. Quant. Electron. **25**, 2634–2639 (1989).
32. M. Kolesik and J. V. Moloney, "Nonlinear optical pulse propagation simulation: From Maxwell's to unidirectional equations," Phys. Rev. E **70**, 036604 (2004).
33. N. A. Panov, D. E. Shipilo, A. M. Saletsky, W. Liu, P. G. Polynkin, and O. G. Kosareva, "Nonlinear transparency window for ultraintense femtosecond laser pulses in the atmosphere," Phys. Rev. A **100**, 023832 (2019).
34. P. A. Oleinikov and V. T. Platonenko, "Raman transitions between rotational levels and self-phase modulation of subpicosecond light pulses in air," Laser Phys. **3**, 618 (1993).
35. W. Liu and S. L. Chin, "Direct measurement of the critical power of femtosecond ti:sapphire laser pulse in air," Opt. Express **13**, 5750 (2005).
36. J. M. Brown, A. Couairon, and M. B. Gaarde, "Ab initio calculations of the linear and nonlinear susceptibilities of n_2, o_2, and air in midinfrared laser pulses," Phys. Rev. A **97**, 063421 (2018).
37. S. A. Akhmanov, V. A. Vysloukh, and A. S. Chirkin, *Optics of femtosecond laser pulses* (1988).
38. J. Kasparian, R. Sauerbrey, and S. L. Chin, "The critical laser intensity of self-guided light filaments in air," Appl. Phys. B **71**, 877 (2000).
39. P. Rairoux, H. Schillinger, S. Niedermeier, M. Rodriguez, F. Ronneberger, R. Sauerbrey, B. Stein, D. Waite, C. Wedekind, H. Wille, L. Wöste, and C. Ziener, "Remote sensing of the atmosphere using ultrashort laser pulses," Appl. Phys. B **71**, 573–580 (2000).